

Optimizing the Preparation Process of Refined Asphalt Based on the Response Surface and Preparation of Needle Coke

Wei Wei and Chenguang Jiang*

Cite This: *ACS Omega* 2024, 9, 13239–13251

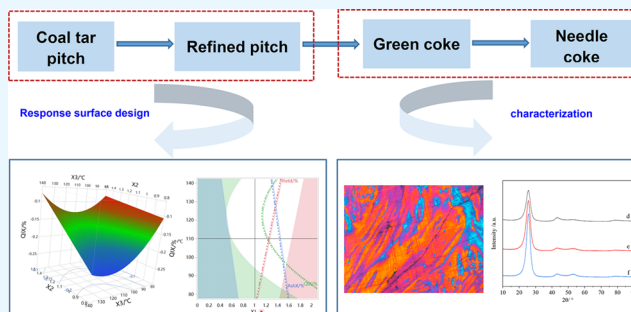
Read Online

ACCESS |

Metrics & More

Article Recommendations

ABSTRACT: Refined asphalt was prepared by solvent extraction sedimentation based on the response surface design, using washing oil and kerosene as solvents and the coal tar pitch as raw materials. The mathematical models of the refined asphalt yield, quinoline insoluble (QI) content, ash content, solvent-to-oil ratio, aromatic-to-aliphatic hydrocarbon ratio, extraction temperature, and sedimentation time were proposed, analyzing the influence of each factor and their interactions on the response values. Therefore, the optimal combination of preparation process parameters and better operation window was obtained by optimizing the experiment. Meanwhile, refined asphalt with high QI content and low QI content was selected as raw material, and the needle coke was prepared through the process of carbonization and calcination. The influence of QI content on the composition and the structure of green coke and needle coke was investigated by X-ray diffraction (XRD), Raman spectra, and polarizing microscopy characterizations. The results showed that the solvent-to-oil ratio is 1.2, aromatic-to-aliphatic hydrocarbon ratio is 1.1, sedimentation time is 2 h, and extraction temperature is 110 °C, resulting in the yield of refined asphalt being 76%, QI content being less than 0.1%, and ash content being less than 0.05%, which meets the requirement of the high-quality needle coke. Otherwise, refined asphalt with lower QI content easily generates a mesophase with more fibers and a large structure in the thermal conversion process, and the corresponding green coke and needle coke have a relatively regular carbon microcrystalline structure.



1. INTRODUCTION

As is well known, pyrolysis is the main method of processing and utilization in the clean transformation process of coal, and a large amount of coal tar is produced as a byproduct. There is an increasing trend of coal tar production year by year in China.¹ Meanwhile, coal tar production in China reached 26.5 million tons in 2021, which made the deep processing of coal tar an urgent problem to be solved. The future development direction of the coal tar industry is centralization, fine separation, deep processing, and synthesis of new materials.² As a heavy component of coal tar, asphalt is usually used as infrastructure materials and heavy fuel oil, resulting in a serious waste of carbon resources and environmental pollution.^{3,4} Asphalt is a mixture of macromolecules with many components and a complex molecular structure, which is composed of polycyclic compounds, thick cyclic aromatics hydrocarbons, and aromatic derivatives.⁵ In addition, as raw materials for preparing high-performance carbon materials, asphalt can be widely used in energy storage, national defense, military, aerospace, and other high-level fields.^{6–8}

In recent years, the gradual development of coal-based carbon materials has attracted the widespread attention of most scholars. As an important carbon material, needle coke has the characteristics of high mechanical strength, high

conductivity, and low thermal expansion efficiency, which can be used to prepare high-power graphite electrodes, lithium-ion battery anode materials, and electrode materials for supercapacitors.^{9–11} The raw materials for needle coke are divided into two types, including oil-based and coal-based. However, the supply of raw materials will be unstable with the increasing shortage of petroleum resources, which will affect the quality of needle coke.¹² Therefore, the development of a coal-based needle coke industry has been promoted based on the energy structure characteristics of rich coal, poor oil, and less gas in China.¹³ Although the production technology of coal-based needle coke has been improving in China, the quality of some needle cokes is equivalent to that of similar foreign products. However, there is still a certain gap compared to foreign high-quality needle coke, such as high-power and ultrahigh-power graphite electrode joint coke, almost all use imported high-

Received: December 14, 2023

Revised: February 21, 2024

Accepted: February 26, 2024

Published: March 7, 2024



quality needle coke. Therefore, “high-end products” and “application differentiation” are the future development directions of the needle coke industry. It is well known that the source and nature of raw materials have important impacts on the quality of coal-based needle cokes,^{14,15} especially for the quinoline insoluble (QI), which is a class of asphalt components with large molecular weight and an extremely complex molecular structure. Asphalt with high QI content has poor fluidity during carbonization and affects the fusion of pellets, which is more likely to generate a spherical mesophase and hinder the formation of a fiber mesophase, resulting in the needle coke with higher mosaic structure content.¹⁶ Therefore, there is a phenomenon in which many researchers pay more attention to the pretreatment process of asphalt.¹⁷

At present, the pretreatment methods for asphalt, including extraction–sedimentation, centrifugation, flash-condensation, extraction–hydrogenation, solvent flocculation, supercritical extraction, etc., have their own advantages and disadvantages.^{18–23} For example, the process of extraction hydrogenation enhanced the coking property of asphalt and easily caused the catalyst deactivation.²⁴ Similarly, the use of flocculants in asphalt pretreatment would introduce new impurities into the product and increase operating costs.²⁵ At present, the method of extraction–sedimentation is accepted by most producing enterprises, but the extraction–sedimentation process has drawbacks such as a big ground occupation area, long sedimentation time, and low efficiency. In this paper, the extraction–sedimentation process is developed to prepare refined asphalt based on the response surface design. It needs to be pointed out that the coal tar pitch of Wuhai Coal Coking Company is used as the raw material, and the commonly used washing oil and kerosene are used as solvent oil. Meanwhile, the models between key factors, including the agent oil ratio, the ratio of aromatic to aliphatic hydrocarbons, sedimentation time, as well as extraction temperature, and the product quality indicators, including yield, QI content, and ash content, were established to improve the efficiency of asphalt pretreatment. Finally, the extraction mechanism of asphalt pretreatment was further revealed, and the influence of asphalt composition on the properties of needle coke was studied. It is meaningful that the group composition of regulation asphalt can be accurately regulated, which is conducive to guiding industrial production.

2. EXPERIMENTAL SECTION

2.1. Experimental Method. In this paper, the preparation technology of refined asphalt was developed based on the response surface design, with the condition that extraction–sedimentation was used to pretreat asphalt, whereas the coal tar pitch of Wuhai Coal Coking Company and washing oil and kerosene were used as the raw material and solvent oil, respectively. First, an appropriate amount of solvent oil and a certain amount of asphalt were successively added to the reactor, and the reaction was stirred at a certain temperature for 1 h so that the asphalt and solvent oil were evenly mixed. Second, the stirring temperature was placed at rest for a period of time after stirring for 1 h so as to settle sufficiently for the insoluble substances. Finally, the discharge port was opened for discharging, and the obtained mixture was distilled to recover the solvent oil in order to obtain the final product, refined asphalt. It should be noted that the extraction–sedimentation device was designed by our laboratory and made by a factory; the discharge port position from the upper end of the reactor height was 75% of the total height of the entire reactor.

Meanwhile, the stirring reaction temperature was the same as the extraction settling temperature.

Refined asphalt with good quality and poor quality was selected as raw material, and the needle coke was prepared through the process of carbonization and calcination. The carbonization experiment was mainly carried out in a sand bath device, the main part of which was independently designed by the laboratory and produced by Beijing Kunlun Yongtai Technology Co., Ltd. Carbonization was carried out under conditions that the heating rate was 5 °C/min, and the temperature increased from room temperature to 490 °C, which was maintained for 2 h at 490 °C. Meantime, the carbonization pressure was 0.5 MPa. When carbonization was completed, the raw coke samples were obtained, and then the needle coke samples were obtained by calcination. Furthermore, the calcination procedure can be described as follows: the heating rate was 5 °C/min, the calcination temperature increased from room temperature to 1200 °C under a N₂ atmosphere, and the N₂ flow rate was 2–3L/min. All of these calcination processes described were carried out in a tubular furnace (GSL-1500X-OTF), which was produced by Hefei Kecrystal Material Technology Co., Ltd.

2.2. Material Characterization. The determination of QI content was done according to the standard GB/T 2293-2019 The method of quinoline-insoluble for pitch products of coal carbonization. The determination of ash content was done according to the standard GB/T 2295-2008 Determination of the ash content of coking solid products. Similarly, the determination of softening points was done according to the standard GB/T 2294-2019 Determination of softening in solid products of coal carbonization. As shown in eq 1, the formula of the yield is as follows:

$$\frac{m_0}{m_1} \times 100\% \quad (1)$$

where m_0 and m_1 represent the quality of asphalt raw material and refined asphalt, respectively.

The crystal structures of the samples were characterized by an X-ray diffractometer (XRD D8 ADVANCE), which was equipped with a Cu target and K α radiation source produced by Bruker Company in Germany. The working voltage and current are 40 kV and 40 mA, respectively. Meantime, the scanning range and rate are 5–80° and 5°/min, respectively. XRD parameter analysis was performed on DIFFRAC.EVA software, and the grain size L_c and L_a of the samples were calculated by eqs 2 and 3.^{26,27}

$$L_c = \frac{K\lambda}{\beta_c \cos \theta_c} \quad (2)$$

$$L_a = \frac{1.84\lambda}{\beta_a \cos \theta_a} \quad (3)$$

where $K = 0.89$; wavelength $\lambda = 0.15406$ nm; β_c and β_a represent the maximum half-peak width (fwhm) of peak 002 and peak 100, respectively; and θ_c and θ_a are the diffraction angles of C(002) and C(100), respectively.

The carbon microcrystalline structure of the samples was determined by a laser confocal Raman spectrometer (LabRam HR-800), which had an incident wavelength of 633 nm, produced by Horiba Jobin Yvon in France.

The polarizing microstructures of samples were observed by a polarizing microscope DM2700 P produced by the German

Table 1. Experimental Factors and Level Settings

inspection factor	code	coding and level					unit
		−1	−	0	+	+1	
solvent-to-oil ratio	X_1	0.80	0.90	1.40	1.80	2.00	dimensionless
aromatic-to-aliphatic hydrocarbon ratio	X_2	0.80	0.90	1.15	1.40	1.50	dimensionless
extraction temperature	X_3	80	89	110	131	140	°C
sedimentation time	X_4	1	1.7	3.5	5.3	6	h

Table 2. DOE Design Matrix and Experimental Results

	X_1	X_2	$X_3/^\circ\text{C}$	X_4/h	yield/%	QI/%	ash/%	QI X/%	ash X/%
1	1.40	1.15	110	3.5	68.30	0.031	0.031	−0.16049	−0.11979
2	1.40	1.15	110	5.3	69.68	0.015	0.014	−0.20993	−0.13896
3	1.40	1.39	110	3.5	67.76	0.045	0.045	−0.13708	−0.10896
4	0.80	1.50	80	6.0	72.30	0.580	0.085	−0.01882	−0.09028
5	0.80	1.50	80	1.0	74.35	0.800	0.160	−0.00748	−0.06978
6	1.40	1.15	110	3.5	70.07	0.039	0.039	−0.14636	−0.11341
7	0.98	1.15	110	3.5	70.93	0.027	0.027	−0.16917	−0.12349
8	0.80	0.80	80	1.0	65.55	0.280	0.065	−0.04715	−0.09848
9	0.80	1.50	140	1.0	71.84	2.390	0.110	−0.02640	−0.08213
10	1.40	1.15	89	3.5	65.15	0.054	0.030	−0.12725	−0.12060
11	2.00	0.80	80	6.0	59.63	0.007	0.007	−0.26887	−0.15701
12	0.80	0.80	140	1.0	70.37	0.054	0.054	−0.12725	−0.10399
13	1.40	1.15	131	3.5	70.09	0.022	0.022	−0.18186	−0.12863
14	2.00	1.50	140	1.0	67.19	0.023	0.023	−0.17951	−0.12770
15	2.00	0.80	140	6.0	62.40	0.003	0.003	−0.34349	−0.17478
16	1.40	1.15	110	1.7	70.20	0.026	0.026	−0.17148	−0.12445
17	2.00	0.80	140	1.0	62.60	0.008	0.007	−0.26201	−0.15512
18	2.00	1.50	140	6.0	66.48	0.028	0.028	−0.16672	−0.12247
19	0.80	0.80	140	6.0	67.80	0.022	0.022	−0.18247	−0.12887
20	0.80	1.50	140	6.0	74.50	2.050	0.105	0.02206	−0.08347
21	1.40	0.90	110	3.5	65.29	0.026	0.022	−0.17148	−0.12887
22	2.00	0.80	80	1.0	61.02	0.110	0.022	−0.08960	−0.12887
23	2.00	1.50	80	6.0	67.43	0.016	0.016	−0.20437	−0.13702
24	1.82	1.15	110	3.5	64.89	0.009	0.009	−0.23955	−0.14857
25	0.80	0.80	80	6.0	64.60	0.490	0.070	−0.02504	−0.09625
26	2.00	1.50	80	1.0	63.69	0.120	0.004	−0.08533	−0.16637

Table 3. Analysis of Variance of the Yield Regression Model

source of variance	sum of squares	degree of freedom	mean square	F	P
model	320.19057	3	106.73000	37.4242	<0.0001
X_1	178.85321	1	178.85321	62.7137	<0.0001
X_2	122.06035	1	122.06035	42.7997	<0.0001
X_3	19.27701	1	19.27701	6.7594	0.0164
residual	62.74179	22	2.85189		
misfitting term	42.84546	11	3.89504	2.1534	0.1095
pure error	19.89632	11	1.80875		
$R^2 = 0.83$					
$R_{\text{Adj}}^2 = 0.81$					
$W = 0.38 > 0.05$					

company LEICA. The sample preparation process can be described in which the samples were fixed in the mold with epoxy resin liquid, and then the samples were polished with 500, 1000, and 2000 grit sandpaper after being fully cured. Meantime, the samples were polished with a 0.05 μm alumina polishing solution. However, it is the best state in which the prepared samples have no significant scratch marks when observed under a 500-fold microscope.

2.3. Experimental Design. The response surface design method can be defined as the experimental scheme was

designed, then the relationship between the investigated factors and the response value was established, and the optimal operation window was obtained by the analysis of the regression equation, all of which were inseparable from software.²⁸ In this paper, the solvent-to-oil ratio, aromatic-to-aliphatic hydrocarbon ratio, extraction temperature, and sedimentation time were selected as impact factors. Otherwise, refined asphalt yield, QI content, and ash content were selected as response values. Meanwhile, the transfer function between the impact factors and the response values was established by

the unconditional jump instruction (JMP) based on the response surface design, which was analyzed by regression. As shown in Table 5, 5 levels were set for each factor, including high and low axial points (coded values +1 and -1), high and low cubic points (coded values + and -), and center points (coded values 0). Meantime, the central point experiment was repeated twice to check the reproducibility of the experiment, which can control the rationality of model fitting and evaluate the pure error of the experiment. It needs to be declared that all experiments were conducted in random order, and JMP software was used for experimental design and analysis, reducing systematic errors.

As shown in Table 1, the experimental combination design of 2 central points with 4 factors and 5 levels was designed based on the central composite. Meanwhile, each factor's influence on the extraction–sedimentation process and the properties of refined asphalt were investigated, as well as the interaction between each factor was analyzed.

3. RESULTS AND DISCUSSION

3.1. Establishing the Regression Model. Based on the response surface optimization experiments, the design of the

Table 4. Analysis of Variance of the QI Regression Model

source of variance	sum of squares	degree of freedom	mean square	F	P
model	0.19563	7	0.02794	26.2140	<0.0001
X_1	0.09787	1	0.09787	91.8046	0.0017
X_2	0.03365	1	0.03365	31.5715	0.0000
X_3	0.01499	1	0.01499	14.0675	0.0000
X_4	0.01154	1	0.01154	10.8268	0.0013
X_3^2	0.01542	1	0.01542	14.4714	0.0015
$X_2 * X_3$	0.01580	1	0.01580	14.8200	0.0040
$X_1 * X_4$	0.00632	1	0.00632	5.9359	0.0254
residual	0.01919	18	0.00106		
misfitting term	0.01909	17	0.00112	11.2548	0.2307
pure error	0.00009	1	0.00010		
$R^2 = 0.91$					
$R_{Adj}^2 = 0.87$					
$W = 0.39 > 0.05$					

Table 5. Analysis of Variance of the Ash Regression Model

source of variance	sum of squares	degree of freedom	mean square	F	P
Model	0.01479	6	0.00246	20.1191	<0.0001
X_1	0.00009	1	0.00009	0.7735	0.0000
X_2	0.00187	1	0.00187	15.2496	0.0009
X_3	0.00043	1	0.00043	3.5289	0.3901
X_4	0.00105	1	0.00105	8.5985	0.1529
$X_2 * X_3$	0.01107	1	0.01107	90.3473	0.0085
$X_2 * X_4$	0.00027	1	0.00027	2.2169	0.0757
residual	0.00232	19	0.00012		
misfitting term	0.00231	18	0.00013	6.2995	0.3050
pure error	0.00002	1	0.00002		
$R^2 = 0.86$					
$R_{Adj}^2 = 0.82$					
$W = 0.38 > 0.05$					

experiment matrix and corresponding experimental results are shown in Table 2. It should be noted that Box–Cox

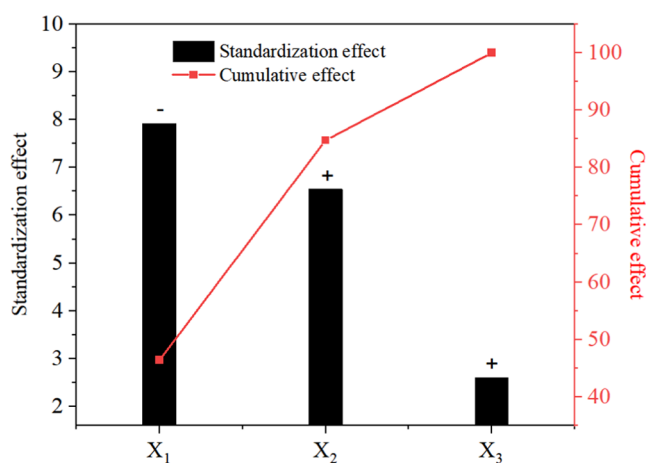


Figure 1. Influence of each factor and its standardization effect on Y_{yield} .

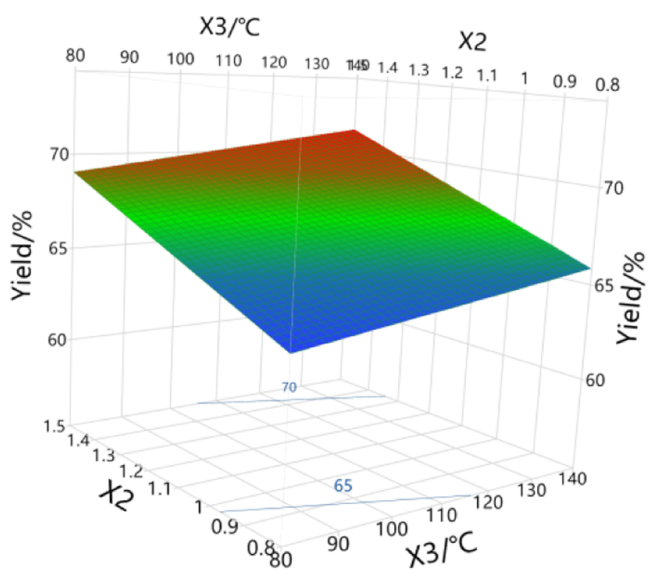


Figure 2. Response surface diagram of $Y_{yield} = f(X_2, X_3)$.

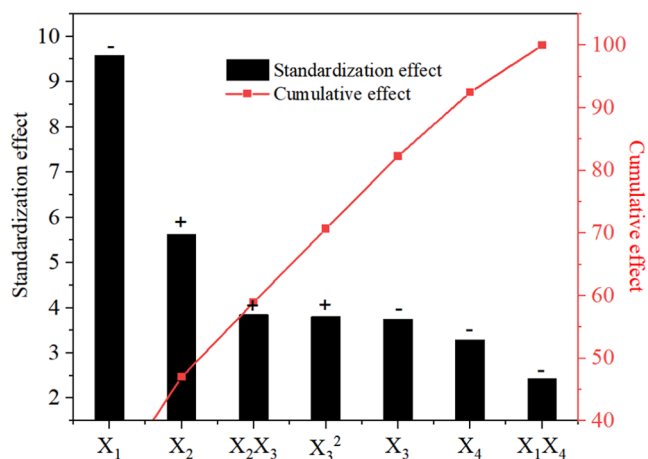


Figure 3. Influence of each factor and its standardization effect on Y_{QIX} .

transformation is carried out for “QI” and “ash”, which are marked as “QI X ” and “ash X ”, respectively, as shown in eqs 4 and 5. As we all know, Box–Cox transformation is a

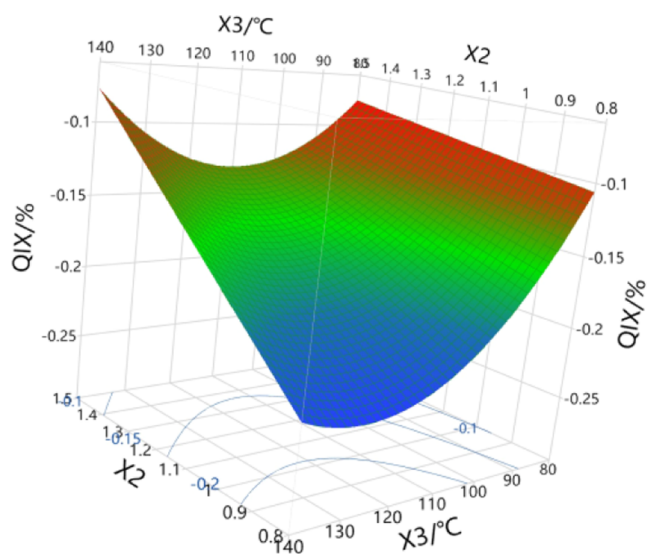


Figure 4. Response surface diagram of $Y_{QIX} = f(X_2, X_3)$.

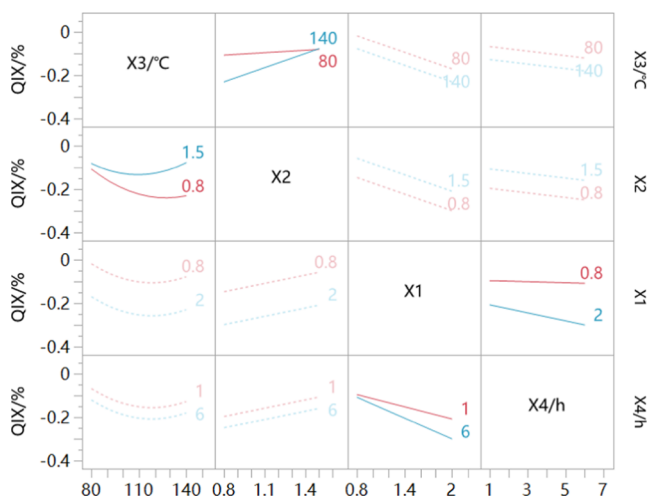


Figure 5. Factor interaction diagram of Y_{QIX} .

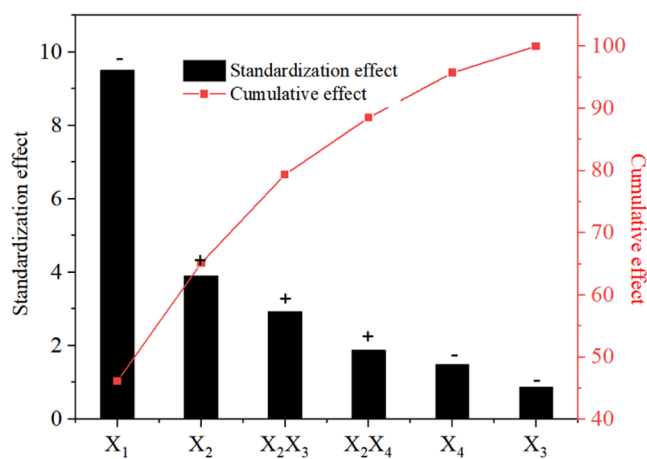


Figure 6. Influence of each factor and its standardization effect on Y_{ashX} .

generalized power transformation method, improving the normality, symmetry, and variance equality of the data, which is used for the condition that continuous response

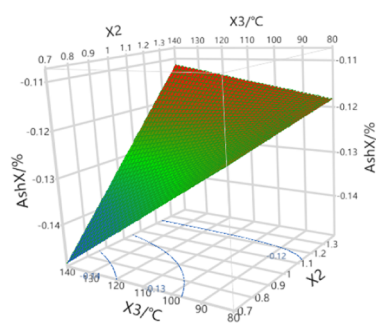


Figure 7. Response surface diagram of $Y_{ashX} = f(X_2, X_3)$.

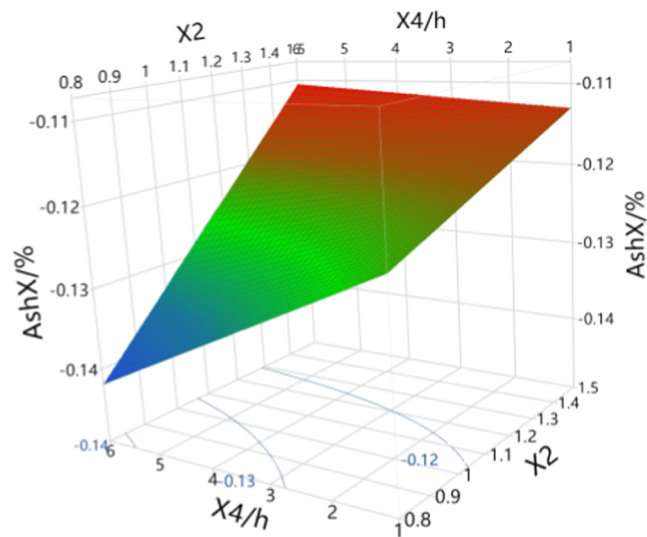


Figure 8. Response surface diagram of $Y_{ashX} = f(X_2, X_4)$.

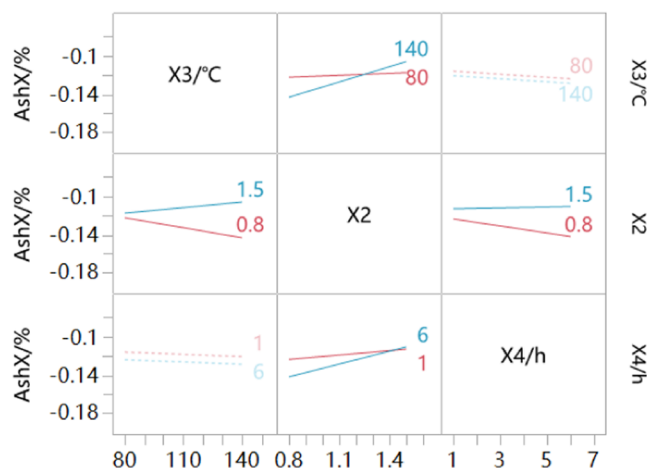


Figure 9. Factor interaction diagram of Y_{ashX} .

variables do not meet the normal distribution. Moreover, the new variable values obtained after transformation are shown in Table 2.

$$QIX = \frac{(QI^{-0.186} - 1)}{-5.6658} \tag{4}$$

$$ashX = \frac{(ash^{0.129} - 1)}{3.0172} \tag{5}$$

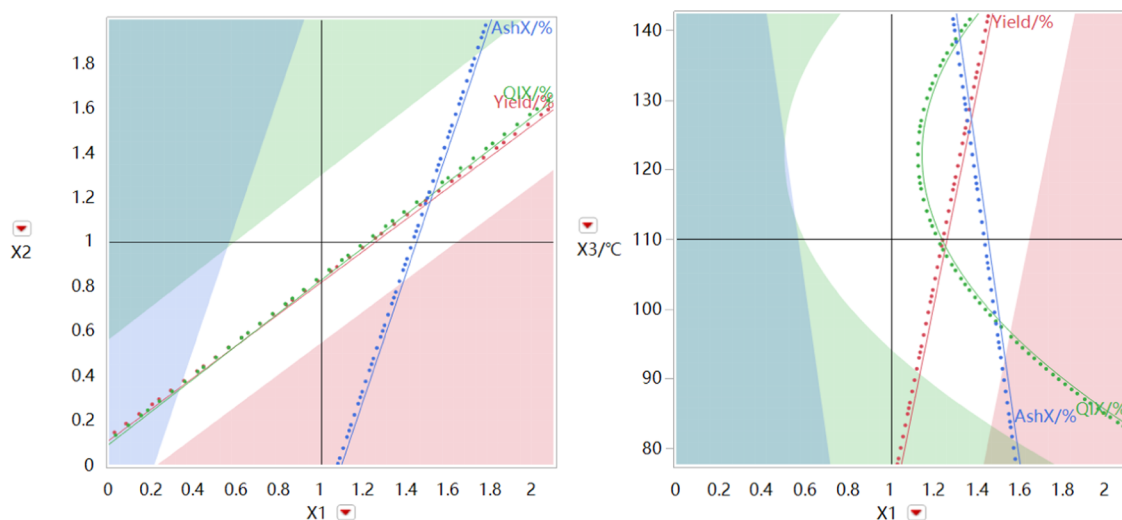


Figure 10. Feasible domain of $Y = f(X_1, X_2)$ and $Y = f(X_1, X_3)$.

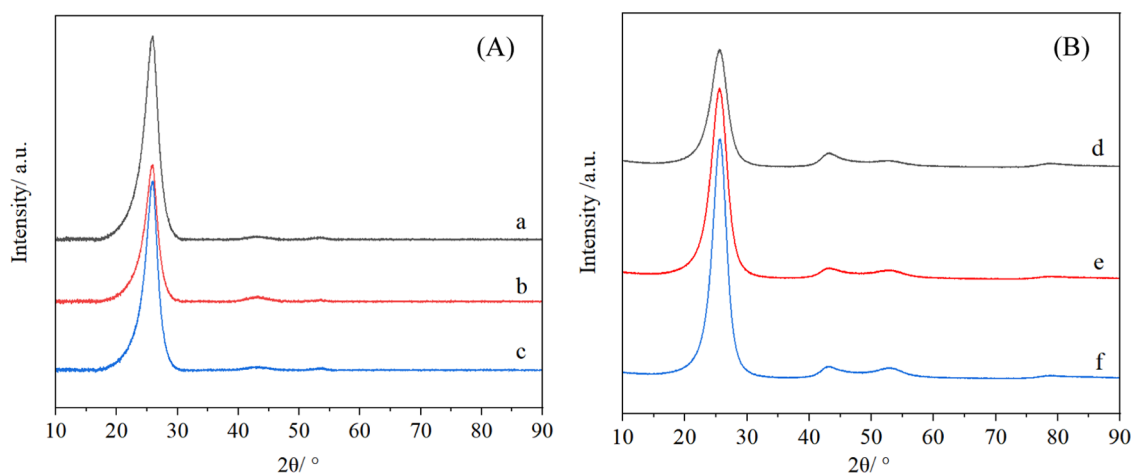


Figure 11. XRD patterns of green coke (A) and needle coke (B). (a) GC0, (b) GC1, (c) GC2, (d) NC0, (e) NC1, and (f) NC2.

It can be seen that the yield range of refined asphalt is 59.63–74.50 wt %, the QI content range is 0.007–2.390 wt %, the ash content range is 0.004–0.160 wt %, and the range of experimental results are wide. Otherwise, the experimental results of groups 1 and 6 are similar, which belong to the central point experiment. All of these results indicate that the experimental design takes more uniform points, and the experimental results are reproducible. Meanwhile, we find that the yield of refined asphalt is limited by the location of the discharge port in the extraction–sedimentation reactor. JMP software was used to fit the experimental results by using the rules of the “stepwise regression method”, “*P*-value threshold”, “backward”, etc. The regression model was established when the parameters were automatically eliminated, with a *P* value less than 0.05.

The responses of yield, QI content, and ash content are labeled as Y_{yield} , Y_{QI} , and Y_{ash} , respectively. Similarly, the impact factors solvent-to-oil ratio, aromatic-to-aliphatic hydrocarbon ratio, extraction temperature, and sedimentation time are labeled as X_1 , X_2 , X_3 , and X_4 , respectively. Therefore, the fitting equation between response values and impact factors can be simplified into eqs 6, 7, and 8.

$$Y_{\text{yield}} = 62.3255 + 0.03549X_3 + 7.6559X_2 - 5.4060X_1 \quad (6)$$

$$Y_{\text{QI}} = -0.0000828 - 0.000990X_3 + 0.127X_2 - 0.126X_1 \\ - 0.0104X_4 + 0.0000595(X_3 - 110)^2 \\ + 0.00299(X_3 - 110)(X_2 - 1.15) \\ - 0.0132(X_1 - 1.4)(X_4 - 3.5) \quad (7)$$

$$Y_{\text{ash}} = -0.0829 - 0.0000787X_3 + 0.0299X_2 - 0.0425X_1 \\ - 0.001599X_4 + 0.000773(X_3 - 110)(X_2 - 1.15) \\ + 0.00594(X_2 - 1.15)(X_4 - 3.5) \quad (8)$$

3.2. Model Variance Analysis. JMP software was used to fit the experimental results, and the adequacy and significance of the model were tested by variance analysis of the yield, QI, and ash regression models. Moreover, the variance analysis of each parameter was carried out by correlation coefficient R^2 , correction correlation coefficient R_{Adj}^2 , *P*-value, residual normality test, *F*-value, and other indices. Usually, the *P*-value can reflect the probability of an event. It can be considered that the parameter is significant, which corresponds

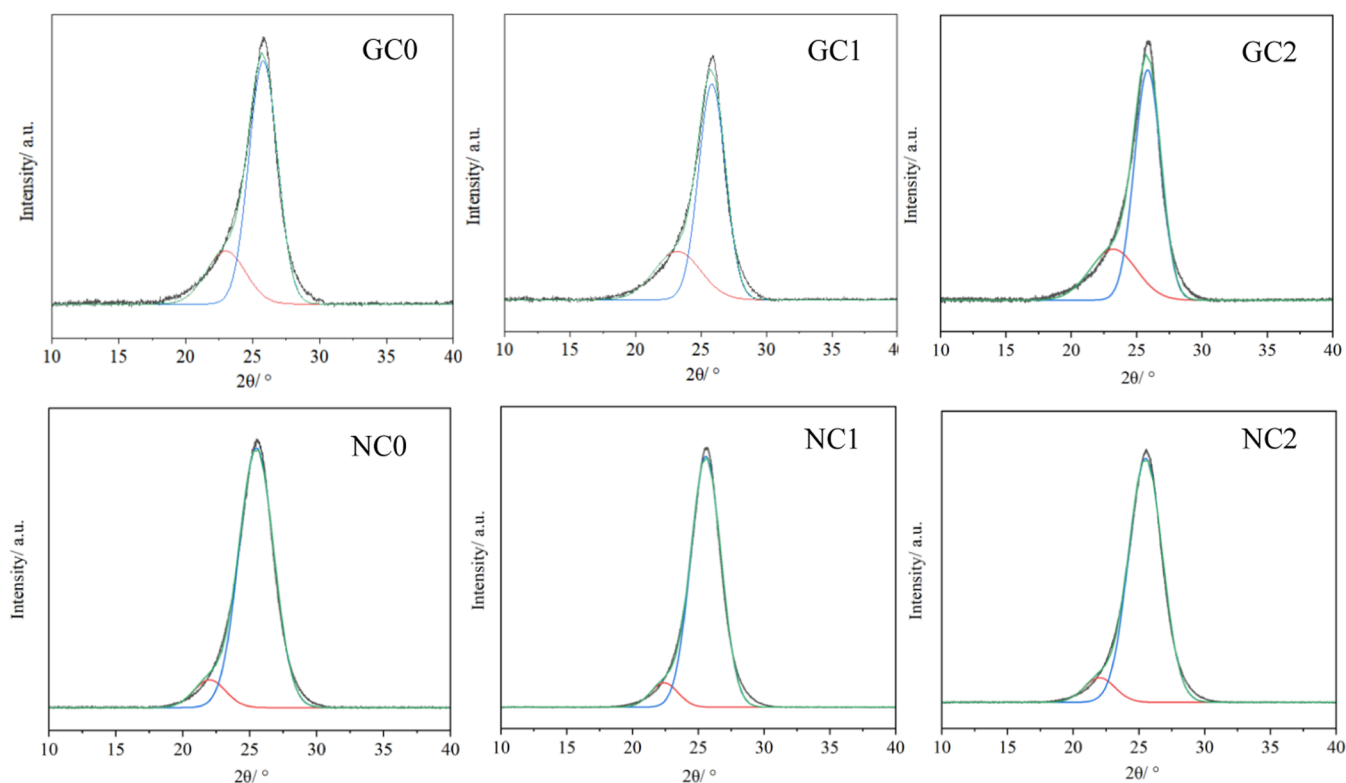


Figure 12. Peak fitting diagram of green coke and needle coke with the XRD diffraction angle 2θ in the range of 20–30°.

Table 6. XRD Parameters of Needle Cokes

sample	$2\theta_{(002)}/^\circ$	$\text{fwhm}_{(002)}/^\circ$	$2\theta_{(100)}/^\circ$	$\text{fwhm}_{(100)}/^\circ$	$d_{002}/\text{\AA}$	$I_g/\%$	$L_c/\text{\AA}$	$L_a/\text{\AA}$
GC0	25.780	2.529	43.136	2.944	3.453	70.83	31.9	59.3
GC1	25.768	2.471	43.182	2.692	3.455	72.15	32.6	64.9
GC2	25.814	2.430	43.524	2.447	3.449	72.26	33.2	71.5
NC0	25.534	2.965	43.160	2.689	3.486	91.11	27.2	64.9
NC1	25.531	2.890	43.204	2.595	3.486	91.60	27.9	67.3
NC2	25.591	2.579	43.054	2.504	3.478	91.89	31.2	69.7

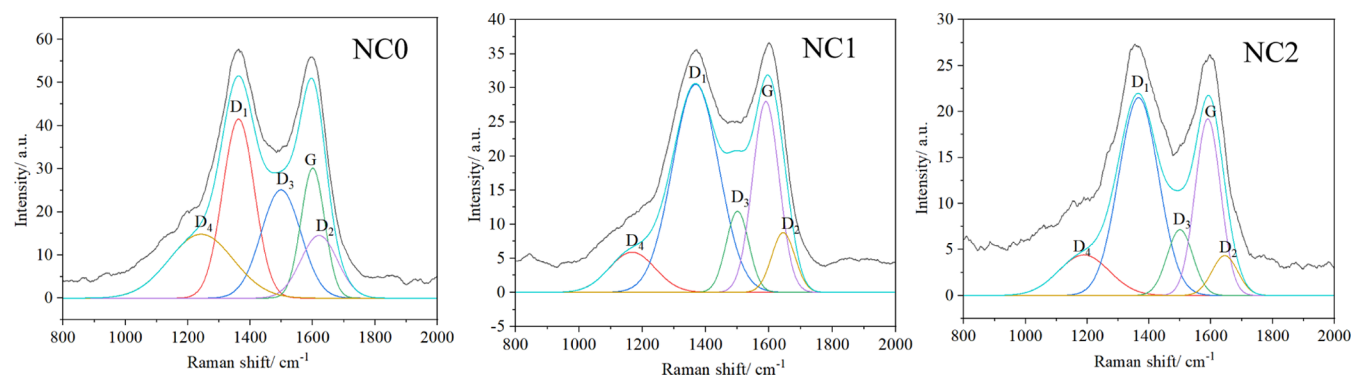


Figure 13. Raman spectrum of needle coke.

to the P -value of less than 0.05. The higher goodness of fit test value of the model (R^2) indicates that the significance of the model can be accepted, and the model does not have the problem of “underfitting”. It can be considered that the model contains correct terms and the model has a high degree of fit and rationality when the values of R^2 and R_{Adj}^2 are close. The residual represents the difference between the predicted values and the measured values.²⁹ The adaptability of the model and the rationality of assumptions can be investigated through a

residual analysis. The goodness of fit test values of the residual distribution $W > 0.05$ indicate that the residual follows a normal distribution and the fitting effect does not depend on some specific values, so the model is real and reliable. However, the model test statistic F -value represents the ratio of variance and residual for the regression model, which, when larger, represents the smaller residual, and the corresponding parameter item has the more significant influence on the model.³⁰

Table 7. Definition of Raman Spectral Characteristic Peaks^{38,39}

band	Raman shift/cm ⁻¹	vibration mode
G	1580	ideal graphitic lattice (E _{2g} symmetry)
D ₁	1350	disordered graphitic lattice (graphene layer edges, A _{1g} symmetry)
D ₂	1620	disordered graphitic lattice (surface graphene layers, E _{2g} symmetry)
D ₃	1500	amorphous carbon (Gaussian line shape)
D ₄	1200	disordered graphitic lattice (A _{1g} symmetry), polyenes, ionic impurities

3.2.1. Variance Analysis of the Yield Model. As shown in Table 3, the *P* value of the regression model of the product yield is significantly less than 0.05, indicating that the model is significant, and the regression model established is suitable for the analysis of product yield. Moreover, the *P* value of the model missing fitting item is 0.1095 > 0.05, indicating that the missing fitting item caused by pure error is not significant and the model has high prediction accuracy. The influence of each factor on the yield of the product was judged according to the *P*-value of each parameter and the corresponding statistic *F*-value. It can be found that the impact factors, including the solvent-to-oil ratio, aromatic-to-aliphatic hydrocarbon ratio, and extraction temperature, have a significant influence on the yield of refined asphalt, and the order of influence is as follows: solvent-to-oil ratio > aromatic-to-aliphatic hydrocarbon ratio > extraction temperature. Meanwhile, the second-order interaction of these impact factors has no effect on the yield of refined asphalt. The correlation coefficient *R*² of the fitted model and the correction determination coefficient *R*_{Adj}² are similar and close to 1. Moreover, it can be seen that the goodness of fit test value of the residual *W* = 0.38 is greater than 0.05, indicating that the residual follows a normal distribution and the reliability of the regression model concerning the “yield” is acceptable.

3.2.2. Variance Analysis of the QI Model. It can be seen from Table 4 that the *P*-value of the QI content model is <0.0001, which is significantly less than 0.05, indicating that the model is significant and the regression model established is suitable for the analysis of the QI content of products. As we all know, the mismatch item can be used to determine whether the model is acceptable for testing and whether the experimental results are statistically significant. However, the *P*-value of the mismatch item is 0.2307 > 0.05, indicating that the model has a high degree of fitting, the predicted value is close to the actual value, as well as the confidence level is less than 95%.³¹ The significance of the influence of the main effect and the interaction effect on QI content was determined by the *P*-value of each parameter item. The larger the *F*-value of the statistic, the more significant the influence of this parameter on the objective function. It can be concluded that the effects of the solvent-to-oil ratio, the aromatic-to-aliphatic hydrocarbon

ratio, extraction temperature, and sedimentation time on the QI content of the product are significant, and the solvent-to-oil ratio > aromatic-to-aliphatic hydrocarbon ratio > extraction temperature > sedimentation time. At the same time, the square effect of extraction temperature, the interaction between the aromatic-to-aliphatic hydrocarbon ratio and extraction temperature, and the interaction between solvent-to-oil ratio and sedimentation time have significant effects on QI content. The correlation coefficient *R*² = 0.91 and the correction determination coefficient *R*_{Adj}² = 0.87 of the model are similar and close to 1, indicating that the model has a high resolution and fitting degree. The goodness of fit test value of the residual error *W* = 0.39 is greater than 0.05, indicating that the residual error follows a normal distribution, the fitting model is reliable, and the fitting effect has nothing to do with the sequence of experiments.

3.2.3. Variance Analysis of the Ash Model. It can be seen from Table 5 that the *P*-value of the model for product ash content is <0.0001, which is significantly less than 0.05, indicating that the model is significant. The regression model established is suitable for the analysis of product refined asphalt ash. The *P*-values of the first-order parameters and second-order interaction terms of the model can be used to determine the significance of the main and interaction effects on the ash content of the product. Moreover, the significant degree of the impact can be judged by the *F*-value of the statistic, and the solvent-to-oil ratio has a significant on the ash content of refined asphalt. The *P*-value of the extraction temperature was 0.3901 > 0.05, and the *F*-value was 3.5289, indicating that the extraction temperature had no significant effect on the ash content of the product. It can be determined that the interaction between the extraction temperature and aromatic-to-aliphatic hydrocarbon ratio has a significant effect on the ash content, according to the *P*-value. Otherwise, according to the *F*-value, ash content is significantly affected by the second-order interaction of the investigated factors, and the interaction between the aromatic-to-aliphatic hydrocarbon ratio and extraction temperature is greater than the interaction between the aromatic-to-aliphatic hydrocarbon ratio and sedimentation time. The values of the correlation coefficient *R*² and correction determination coefficient *R*_{Adj}² are very close to 0.9, indicating that the regression model has good prediction accuracy and rationality.

3.3. Response Surface Analysis of the Regression Model. It can be seen from the variance analysis of the regression model that the influence of each factor on the yield, QI content, and ash content is not a simple linear relationship but a curved surface relationship. The influence of each factor and the interaction between the factors on the response values were analyzed by the factor interaction diagram, surface diagram, and Pareto diagram so as to further analyze the asphalt extraction mechanism. The surface diagram describes the change trend of the response value affected by the change

Table 8. Parameters of Curve-Fitted Raman Spectra^{a,b}

sample	fwhm/cm ⁻¹					area/10 ⁵									
	D ₁	D ₂	D ₃	D ₄	G	I _{D1}	I _{D2}	I _{D3}	I _{D4}	I _G	I _G /I _{All}	I _{D1} /I _G	I _{D2} /I _G	I _{D3} /I _G	I _{D4} /I _G
NC0	120	138	149	242	89	5313	2136	3995	3822	2857	0.16	1.86	0.75	1.40	1.34
NC1	172	86	84	169	98	5616	807	1067	1613	2932	0.26	1.91	0.27	0.36	0.55
NC2	148	83	79	229	96	4551	699	984	1072	2977	0.27	1.53	0.23	0.33	0.36

^aI_{D1}, I_{D2}, I_{D3}, I_{D4}, and I_G represent the integral values of peak areas, respectively. ^bI_{All} represents the integral value of the total area.

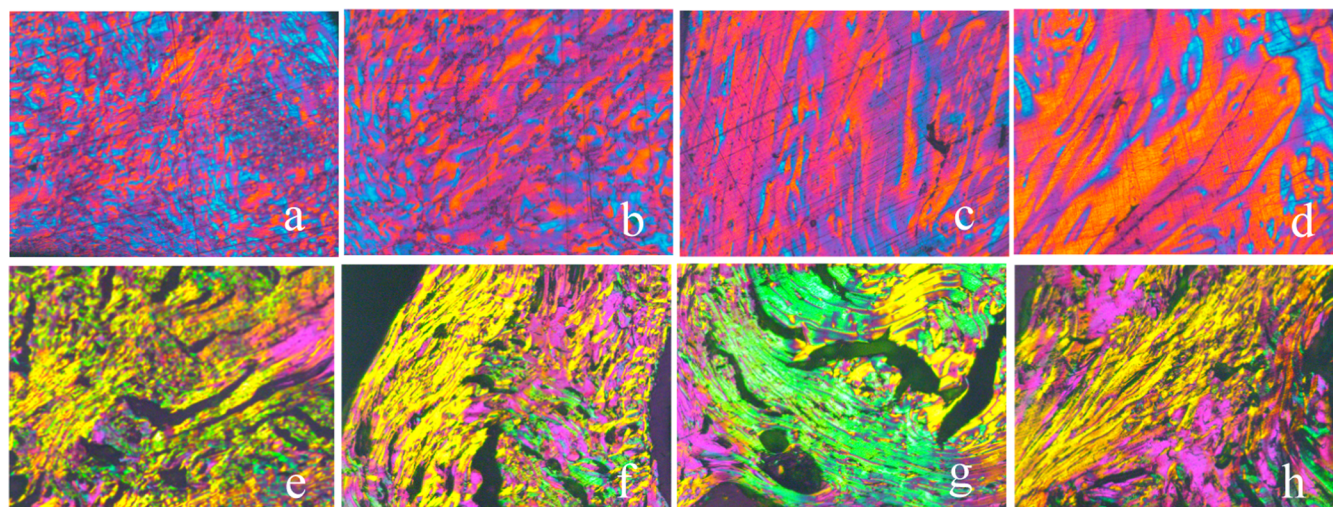


Figure 14. Polarized light optical micrographs of green coke and needle coke. (a, b) GC1, (c, d) GC2, (e, f) NC1, and (g, h) NC2.

Table 9. Polarized Structural Content of Green Coke GC1 and GC2

	mosaic/%	wide domain streamline/%	short fiber/%	long fiber/%	isotropy no optical properties/%	total anisotropic structure content/%
GC1	3.92	7.86	1.20	1.34	85.68	14.32
GC2	0.78	86.82	3.10	9.30	0	100

of the two factors when the other two factors are at the central level.³² The factor interaction diagram describes the change trend of the response value caused by another factor changes from a low level to a high level when one factor is at a low or high level, whereas the dotted line is the parallel line, indicating that the two factors have no interaction, and the solid line indicates that the two factors have interaction. The Pareto diagram can describe independent variables and the normalization effect between them, in which the column length represents the normalization effect of each parameter term on the response, including the first term, the second term, and their cross terms.^{33,34} Moreover, the greater the standardization effect, the more significant the influence of the parameter item. It needs to be noted that the positive and negative signs at the top of each bar chart represent the positive and negative values of the estimated values of the corresponding parameters.

3.3.1. Response Surface Analysis of the Yield Model. It can be seen from Figure 1 that the yield of refined asphalt is most affected by the ratio of solvent-to-oil in the reaction system, followed by the aromatic-to-aliphatic hydrocarbon ratio and extraction temperature. Meanwhile, the influence of the linear term of the investigated factors is significant, indicating that the fitted model has a certain linear relationship but no surface relationship, so there is no factor interaction graph. In addition, it can be seen from Figure 2 that the interaction between the aromatic-to-aliphatic hydrocarbon ratio and extraction temperature and the yield of response value present an inclined plane relationship, indicating that the yield of response value changes linearly with the ratio of aromatic-to-aliphatic hydrocarbon and extraction temperature. The ratio of solvent-to-oil is large, which means that the amount of solvent oil used is more, and the solubility of asphalt increases, causing the viscosity of the whole reaction system to decrease. Meantime, asphalt with a large molecular weight is more likely to precipitate. Therefore, the ratio of solvent-to-oil and the yield of refined asphalt show a negative correlation.

3.3.2. Response Surface Analysis of the QI Model. It can be seen from Figure 3 that the ratio of solvent-to-oil has the greatest influence on the QI content of refined asphalt. For the investigated factors, the linear term accounted for 68.81%, the square term accounted for 11.76%, and the cross term accounted for 19.43%. It is shown in Figure 4 that the ratio of solvent-to-oil in the system and the interaction of investigated factors have significant effects on QI content, and the fitting model shows a curved surface relationship. The ratio of solvent-to-oil is negatively correlated with the content of QI in refined asphalt products, indicating that the increase in the use of solvent oil can reduce the QI content in products, which may be caused by the viscosity and density of the reaction system being reduced, and the fluidity of the system is enhanced, and all of these results are conducive to the removal of QI. There is a positive correlation between the ratio of aromatic-to-aliphatic hydrocarbon and QI content because the larger the ratio of aromatic-to-aliphatic hydrocarbon in the mixed solvent, the stronger the solubility of asphalt in the mixed solvent, resulting in a less heavy phase being formed. Therefore, the fine QI particles cannot be brought out during sedimentation separation, resulting in a higher QI content in the refined asphalt. However, it can be seen from Figure 5 that the viscosity of the reaction system decreased with the increase of extraction temperature when the ratio of aromatic-to-aliphatic hydrocarbon is constant, which is conducive to the sedimentation and separation of QI, resulting in the decrease of QI content in the refined asphalt. It is interesting that the QI content increased with the increase of extraction temperature when the extraction temperature was higher than 130 °C, which may be due to the fact that the higher extraction temperature caused some of the organic compounds with larger molecular weight in the asphalt to dissolve and disperse into the supernatant, resulting in a reduction in the separated QI. It can be concluded that the interaction between extraction temperature and aromatic-to-aliphatic hydrocarbon ratio has a

significant impact on QI content of the products, showing a curved surface relationship.

3.3.3. Response Surface Analysis of the Ash Model. The composition of QI can be divided into inorganic substances and organic particles. Organic macromolecular particles are mainly derived from the cracking of high-molecular-weight aromatic hydrocarbons of coal or from the high condensation of the polyaromatic ring, which is formed by thermal polymerization of aromatic hydrocarbon with a small molecular weight of the cracking product at high temperature. Meanwhile, most of the organic particles are composed of micrometer carbon particles with amorphous carbon similar to the structure of carbon black. Otherwise, the ash content of inorganic particles is high, which is mainly composed of ash particles derived from raw coal and the residual catalyst. Therefore, the content of QI in refined asphalt has a certain correlation with the content of ash.

It can be seen from Figure 6 that the solvent-to-oil ratio has the most significant effect on the ash content of the refined asphalt, followed by the ratio of aromatic-to-aliphatic hydrocarbon. As for the standardization effect, the proportion of the linear term of the ratio of solvent-to-oil, aromatic-to-aliphatic hydrocarbon, extraction temperature, and sedimentation time is 76.52%, and the proportion of the interaction term is 23.48%. Although the fitting model mainly presents a primary relationship, it represents a surface relationship in general. The ratio of solvent-to-oil is negatively correlated with the ash content in refined asphalt, which is consistent with the QI content in refined asphalt. The viscosity of the reaction system decreased, and the fluid fluidity increased due to the large amount of solvent oil used. Meantime, according to the Stokes theorem (eq 9), the increase of particles enhances the collision frequency of small granular inorganic matter and the aggregation frequency of inorganic matter particles and heavy residue in the system, making ash particles easy to precipitate while taking away part of the heavy hydrocarbon insoluble residue in the raw material, all of which leads to the reduction of ash content and yield in the refined asphalt as well as the QI content.³⁵

$$\mu_t = \frac{g(\rho_p - \rho)D_p^2}{18\mu} \quad (9)$$

where μ_t is the settling velocity of particles, g is the gravitational acceleration, D_p is the radius of the particles, ρ and ρ_p represent the specific gravity of the particles, and μ is the viscosity of the solution medium.

As we all know, the increase in the ratio of aromatic-to-aliphatic hydrocarbon means that the usage amount of aromatic hydrocarbon solvent washing oil is increased and the proportion of paraffin solvent kerosene is reduced. According to the principle of similar phase dissolution, the solubility of the washing oil to the asphalt in the reaction system is large, and kerosene can accelerate the flocculation of macromolecular insoluble matter. Therefore, the increase in the aromatic-to-aliphatic hydrocarbon ratio leads to the increase in the ash content in refined asphalt, which may be due to two reasons. On the one hand, the settling velocity of particles decreases due to the reduction in the density difference ($\rho_p - \rho$) between the particles and the mixed liquid. On the other hand, the precipitation phase in the mixed system is relatively small, and the solution tends to be evenly distributed, which makes the small particles of ash not easy to

aggregate and settle. As shown in Figure 9, the ash content in products decreases with the increase in the extraction temperature when the aromatic-to-aliphatic hydrocarbon ratio is 0.8, which may be due to the solubility of solvent oil to asphalt raw materials being small, and the viscosity of the reaction system being large, under the condition of a relatively small aromatic-to-aliphatic hydrocarbon ratio. Meanwhile, the increase in extraction temperature can reduce the viscosity of the system and increase the fluid flow, which is conducive to the settlement of ash particles. Similarly, the increase of sedimentation time under this aromatic-to-aliphatic hydrocarbon ratio is conducive to the full sedimentation of particles and the reduction of the ash content of products. However, the amount of an alkane solvent in the reaction system is less, and the viscosity of the system is lower under the aromatic-to-aliphatic hydrocarbon ratio of 1.5. The viscosity of the system reduced and was difficult to reach the supersaturation state due to the increase in the extraction temperature. Furthermore, the ash dispersion of small particles is relatively uniform and difficult to gather, so the ash content in refined asphalt increases. At the same time, the increase in sedimentation time under this condition has no effect on the sedimentation of smaller ash particles, so the ash content in the product has almost no change with the increase in sedimentation time. Therefore, as shown in Figures 7 and 8, the interaction between the aromatic-to-aliphatic hydrocarbon ratio and extraction temperature and the interaction between the aromatic-to-aliphatic hydrocarbon ratio and sedimentation time show a curved relationship with the ash content in the products (Figure 9).

3.4. Multiobjective Optimization. As we all know, the ash content of the performance index of high-grade needle coke is <0.2%, and it is expected that the yield of refined asphalt is no less than 60 wt % based on economic considerations. Meanwhile, the refined asphalt with high QI content is not conducive to the formation of streamlined mesophase asphalt, thus affecting the quality of the product needle coke. In this work, it is expected that the QI content of refined asphalt is no more than 0.1%. Therefore, the upper and lower limits of the three response values can be obtained, and the optimal preparation process parameters are obtained by setting and maximizing the predictive profiler. The optimal preparation parameters were selected as the ratio of solvent-to-oil is 1.2, the ratio of aromatic-to-aliphatic hydrocarbon is 1.1, the sedimentation time is 2 h, and the extraction temperature is 110 °C, combined with the actual operation conditions. Correspondingly, the yield of refined asphalt is 76%, the QI content is less than 0.1%, and the ash content is less than 0.05%.

Based on the optimal combination of process parameters, 5000 Monte Carlo simulations were carried out to calculate the complex process capability index (Cpk) of the analytical model, which can be calculated by eq 10. It should be noted that the Cpk represents the degree to which the manufacturing process meets the production requirements. Usually, the larger the Cpk value, the better the processing quality. Among them, the Cpk of yield is 1.531, the Cpk of QI content is 1.197, and the Cpk of ash content is 1.514, all of which are greater than 1, indicating that the models have strong process capability and reliable model quality.

$$Cpk = \min\left(\frac{\mu - LSL}{3\sigma}, \frac{USL - \mu}{3\sigma}\right) \quad (10)$$

where μ represents the average of actual values; USL and LSL represent the upper and lower specification limits of the actual value, respectively; and σ represents the standard deviation of the actual value.

As shown in Figure 10, the ratio of solvent-to-oil and the ratio of aromatic-to-aliphatic hydrocarbon, which are easy to control in daily operation, are taken as variables, and other factors, including an extraction temperature of 110 °C and a sedimentation time of 1 h, are all fixed levels. It is especially explained that the white area is the operable interval of the ratio of solvent-to-oil and the ratio of aromatic-to-aliphatic hydrocarbon. Similarly, when the ratio of aromatic-to-aliphatic hydrocarbon is 1 and the sedimentation time is 1 h, the extraction temperature and the ratio of solvent-to-oil are the operating variables, where the operable interval is the white area.

3.5. Characterization of Green Coke and Needle Coke. The green coke was obtained by the carbonization of the asphalt raw material, the refined asphalt with high QI content, and the refined asphalt with low QI content, which was labeled as GC0, GC1, and GC2, respectively. Furthermore, the needle coke was obtained by the calcination of the green coke, which was labeled as NC0, NC1, and NC2, respectively. It needs to be explained that the refined asphalt with high QI content and the refined asphalt with low QI content are selected from the DOE design matrix products, which are the group 20 and group 2 experimental products, respectively. The influence of asphalt raw material composition on the quality of needle coke can be determined by the characterization analysis of green coke and needle coke, including XRD, polarizing microstructure analysis, and Raman characterizations, which are conducive to the accurate control of asphalt raw material composition.

The X-ray diffraction characterization results of green and needle coke are presented in Figure 11. It can be found that the green coke and needle coke prepared present a large 002 peak with a complete peak shape, indicating that the carbon microcrystalline structure in the prepared carbon material tends to be complete. As reported by Manoj,²⁶ the X-ray diffraction peak (002) of the samples for the nongraphitized carbon-rich material shows the superposition of the carbon peaks of the amorphous structure and the carbon microcrystal peaks of the regular structure; the corresponding positions are about 22 and 26°, and the corresponding peak areas of the two are labeled as I_{22} and I_{26} , respectively. As shown in Figure 12, the area of the two carbon peaks can be calculated by fitting the subpeaks of the (002) peaks, and thus, the content of the neatly arranged carbon microcrystals I_g in the carbon-rich material can be obtained. I_g is calculated from eq 11.

$$I_g = I_{26}/(I_{22} + I_{26}) \quad (11)$$

Among them, I_{22} represents the area of amorphous carbon peaks and I_{26} represents the area of peaks of carbon microcrystals with an arrangement that tends to be a regular structure.

The microcrystalline structure parameters of green coke and needle coke were calculated by eqs 2 and 3, and the content of microcrystalline carbon was calculated by eq 11. Meanwhile, the calculation results are shown in Table 6.

It can be seen that microcrystalline size in the C-axis direction L_c , the horizontal diameter of carbon microcrystalline L_a , and the content of carbon microcrystalline I_g are in the order of GC2 > GC1 > GC0, and NC2 > NC1 > NC0. As we

all know, the smaller L_c indicates that the carbon layer of needle coke is more chaotic. Therefore, the carbon layer of green coke and needle coke prepared from untreated asphalt is the most chaotic, which is in agreement with the calculated carbon content of graphite microcrystalline. In addition, as shown in Table 6, the horizontal diameters of carbon microcrystal L_a of GC2 and NC2 samples are the largest, indicating that its graphitization degrees are high and the carbon layers are more regular.

The Raman spectra of the prepared needle coke are presented in Figure 13, and there are D and G peaks in the range of the 800–2000 cm^{-1} shift for the three cokes. As we all know, the presence of the D peak indicates that there are more amorphous carbons and irregular microcrystalline carbons in carbon materials.³⁶ Therefore, in this work, the first-order Raman spectra of carbon-rich materials were studied by using the mathematical method of split-peak fitting, and the differences in forms of carbon microcrystals in carbon-rich materials were revealed, as shown in Figure 13. There are five carbon peaks, including D1, D2, D3, D4, and G, in the peak fitting results of all prepared needle cokes. As shown in Table 7, D1, D2, D3, and D4 peaks belong to the defect peaks of carbon microcrystals. The larger the I_G/I_{All} ratio of the G peak area, the smaller the ratio of the defect peak area to G peak, which refers to the values of I_{D1}/I_G , I_{D2}/I_G , I_{D3}/I_G , and I_{D4}/I_G . In other words, the smaller the defect of carbon microcrystals, the more regular the arrangement for the carbon materials. As shown in Table 8, it can be found that the value of I_G/I_{All} follows: NC2 > NC1 > NC0, and the ratio of the defect peak area to G peak area shows an opposite trend.³⁷ Therefore, the needle coke prepared from the refined asphalt with a low QI content has a relatively regular carbon microcrystalline structure, and the analysis results are consistent with the XRD analysis results.

The polarized light optical micrographs of green coke and needle coke are presented in Figure 14. As shown in Figure 14a–d, the green coke prepared presents part of a large area of an anisotropic structure with good orientation, especially as shown in Figure 14c,d, with a large drainage basin structure, which is conducive to gas coke drawing and forming a large area of an orderly “needle bundle” organizational structure.⁴⁰ However, the green coke GC1 has some isotropic structure and a more mosaic structure, which should be due to the fact that the asphalt with higher QI content is easy to generate a mesophase with a mosaic structure in the thermal conversion process.⁴¹ Meanwhile, the polarized structural content of green coke GC1 and GC2 is shown in Table 9, which was calculated by the polarization microscopy quantitative analysis method.⁴² The mesophase content of green coke GC2 is higher than that of green coke GC1, which is consistent with the content of a wide domain streamline. In addition, as shown in Figure 14e–h, the needle cokes NC0 and NC1 have a more mosaic structure, and the needle coke NC2 has a more fiber structure and a large structure, which are consistent with the polarized light optical micrographs of green coke.

4. CONCLUSIONS

In this work, the effects of extraction temperature, sedimentation time, the ratio of solvent-to-oil and aromatic-to-aliphatic hydrocarbon ratio on the yield, QI content, and ash content of the refined asphalt were studied by response surface analysis. Therefore, models were established to investigate the relationship between the factors and response

values, including yield, QI content, and ash content. It was found that the regression models have high fit and reliable quality by the analysis of variance and process capability. Moreover, the influence of the solvent-to-oil ratio on the refined asphalt yield, QI content, and ash content is more significant, followed by the ratio of aromatic-to-aliphatic hydrocarbon, according to the analysis of the Pareto diagram, factor interaction diagram, and response surface diagram. The refined asphalt of QI content and ash content were significantly affected by the interaction between the ratio of aromatic-to-aliphatic hydrocarbon and extraction temperature. In short, the optimal combination of preparation process parameters was obtained by analysis of regression models, and refined asphalt with high quality was prepared. Furthermore, needle coke can be easily obtained by carbonization and calcination of refined asphalt with a lower QI content, which has a higher content of carbon microcrystals with regular arrangement and a large area of an orderly “needle bundle” structure.

AUTHOR INFORMATION

Corresponding Author

Chenguang Jiang – National Institute of Clean and Low Carbon Energy, Beijing 102211, China; orcid.org/0000-0002-4270-6533; Phone: +86 10 57337583; Email: jiangcg521@126.com

Author

Wei Wei – China Energy Coal Coking Company, Wuhai 016030, China

Complete contact information is available at: <https://pubs.acs.org/10.1021/acsomega.3c10019>

Notes

The authors declare no competing financial interest.

ACKNOWLEDGMENTS

This work was supported by a grant from the National Energy Investment Group Technology Innovation Project of China (No. S930023054).

REFERENCES

- (1) Diez, M. A.; Garcia, R. *New Trends in Coal Conversion*; Wood Head Publishing: New York, 2019.
- (2) Ma, Z.; Wei, X.; Liu, G.; Liu, F.; Zong, Z. Value-added utilization of high-temperature coal tar: A review. *Fuel* **2021**, *292* (6), No. 119954, DOI: [10.1016/j.fuel.2020.119954](https://doi.org/10.1016/j.fuel.2020.119954).
- (3) You, Z.; Xiao, J.; Wang, G.; Yao, Z.; Wan, Y.; Zhong, Q. Molecular representation and atomic-level coking evolution investigation of modified coal tar pitch via ¹³C NMR, MALDI-TOF-MS, SAXS, and ReaxFF MD. *Fuel* **2023**, *348*, No. 128561, DOI: [10.1016/j.fuel.2023.128561](https://doi.org/10.1016/j.fuel.2023.128561).
- (4) Tian, Y.; Huang, Y.; Yu, X.; Gao, F.; Gao, S.; Wang, F.; Li, D.; Xu, X.; Cui, L.; Fan, X.; Dong, H.; Liu, J. Co-carbonization of medium and low temperature coal tar pitch and coal-based hydrogenated diesel oil prepare mesophase pitch for needle coke precursor. *Adv. Eng. Mater.* **2021**, *23* (10), No. 2001523, DOI: [10.1002/adem.202001523](https://doi.org/10.1002/adem.202001523).
- (5) Zhang, Z.; Wang, Z.; Zhang, L.; Guo, S.; Ji, H.; Liu, Y.; Zhao, G.; Zhu, W.; Jiao, C.; Cao, Y.; Liu, D. Study on the co-carbonization behavior of high-temperature coal tar pitch and raffinate oil of low-temperature coal tar. *Fuel* **2022**, *310*, No. 122469, DOI: [10.1016/j.fuel.2021.122469](https://doi.org/10.1016/j.fuel.2021.122469).
- (6) Lv, J.; Bai, H.; Zhu, Y.; Hu, C.; Xu, Y.; Lai, S.; Zhao, X. Synthesis and characterization of mesophase coke from medium–low-temperature coal tar pitch modified by high-pressure thermal polymerization. *Asia-Pac. J. Chem. Eng.* **2021**, *16* (4), No. e2643, DOI: [10.1002/apj.2643](https://doi.org/10.1002/apj.2643).
- (7) Liu, Y.-C.; Hung, Y.-H.; Sutarsis; Hsu, C.-C.; Ni, C.-S.; Liu, T.-Y.; Chang, J.-K.; Chen, H.-Y. Effects of surface functional groups of coal-tar-pitch-derived nanoporous carbon anodes on microbial fuel cell performance. *Renewable Energy* **2021**, *171* (7), 87–94, DOI: [10.1016/j.renene.2021.01.149](https://doi.org/10.1016/j.renene.2021.01.149).
- (8) Yang, Y.; Zuo, P.; Qu, S. Adjusting hydrophilicity and aromaticity strategy for pitch-based hierarchical porous carbon and its application in flexible supercapacitor. *Fuel* **2022**, *311*, No. 122514, DOI: [10.1016/j.fuel.2021.122514](https://doi.org/10.1016/j.fuel.2021.122514).
- (9) Zhang, Z.; Huang, X.; Zhang, L.; Guo, S.; Du, H.; Chen, Z.; Wu, B.; Li, G.; Liu, D. Study on the evolution of oxygenated structures in low-temperature coal tar during the preparation of needle coke by co-carbonization. *Fuel* **2022**, *307*, No. 121811, DOI: [10.1016/j.fuel.2021.121811](https://doi.org/10.1016/j.fuel.2021.121811).
- (10) Li, X.; Zhao, L.; He, T.; Zhang, M.; Wang, Z.; Zhang, B.; Weng, X. Highly conductive, hierarchical porous ultra-fine carbon fibers derived from polyacrylonitrile/ polymethylmethacrylate/ needle coke as binder-free electrodes for high-performance supercapacitors. *J. Power Sources* **2022**, *S21*, No. 230943, DOI: [10.1016/j.jpowsour.2021.230943](https://doi.org/10.1016/j.jpowsour.2021.230943).
- (11) Lee, S. E.; Kim, J. H.; Lee, Y.-S.; Im, J. S. Effect of coke orientation on the electrochemical properties of lithium-ion battery anode. *J. Appl. Electrochem.* **2021**, *51* (10), 1407–1418, DOI: [10.1007/s10800-021-01581-x](https://doi.org/10.1007/s10800-021-01581-x).
- (12) Lin, X.; Sheng, Z.; He, J.; He, X.; Wang, C.; Gu, X.; Wang, Y. Preparation of isotropic spinnable pitch with high-spinnability by co-carbonization of coal tar pitch and bio-asphalt. *Fuel* **2021**, *295*, No. 120627, DOI: [10.1016/j.fuel.2021.120627](https://doi.org/10.1016/j.fuel.2021.120627).
- (13) Li, J.; Tian, Y.; Yan, X.; Yang, J.; Wang, Y.; Xu, W.; Xie, K. Approach and potential of replacing oil and natural gas with coal in China. *Front. Energy* **2020**, *14* (2), 419–431, DOI: [10.1007/s11708-020-0802-0](https://doi.org/10.1007/s11708-020-0802-0).
- (14) Zhang, Z.; Du, H.; Guo, S.; Lou, B.; Yu, R.; Gong, X.; Li, Z.; Li, M.; Duan, Y.; Yuan, H.; Liu, D. Probing the effect of molecular structure and compositions in extracted oil on the characteristics of needle coke. *Fuel* **2021**, *301*, No. 120984, DOI: [10.1016/j.fuel.2021.120984](https://doi.org/10.1016/j.fuel.2021.120984).
- (15) Zhang, Z.; Lou, B.; Zhao, N.; Yu, E.; Wang, Z.; Du, H.; Chen, Z.; Liu, D. Co-carbonization behavior of the blended heavy oil and low temperature coal tar for the preparation of needle coke. *Fuel* **2021**, *302*, No. 121139, DOI: [10.1016/j.fuel.2021.121139](https://doi.org/10.1016/j.fuel.2021.121139).
- (16) Zhu, Y.; Liu, H.; Xu, Y.; Hu, C.; Zhao, X. Preparation and characterization of coal-pitch-based needle coke (Part III): the effects of quinoline insoluble in coal tar pitch. *Energy Fuels* **2020**, *34* (7), 8676–8684, DOI: [10.1021/acs.energyfuels.0c01049](https://doi.org/10.1021/acs.energyfuels.0c01049).
- (17) Jiao, S.; Guo, A.; Wang, F.; Yu, Y.; Biney, B. W.; Liu, H.; Chen, K.; Liu, D.; Wang, Z.; Sun, L. Sequential pretreatments of an FCC slurry oil sample for preparation of feedstocks for high-value solid carbon materials. *Fuel* **2021**, *285*, No. 119169, DOI: [10.1016/j.fuel.2020.119169](https://doi.org/10.1016/j.fuel.2020.119169).
- (18) Lin, X.; Li, S.; Guo, F.; Jiang, G.; Chen, X.; Wang, Y. High efficiency extraction and modification on the coal liquefaction residue using supercritical fluid with different types of solvents. *Energy Fuels* **2016**, *30* (5), 3917–3928, DOI: [10.1021/acs.energyfuels.6b00326](https://doi.org/10.1021/acs.energyfuels.6b00326).
- (19) Lu, C.; Li, D.; Wang, L.; Fan, A.; Cui, W.; Li, W. Combined filtration and electric desalination for coal tar pretreatment. *Energy Sources, Part A* **2018**, *40* (7), 854–861, DOI: [10.1080/15567036.2018.1463316](https://doi.org/10.1080/15567036.2018.1463316).
- (20) Li, L.; Wang, Y.; Lin, X.; Lv, J.; He, J.; Zhang, Y. Effect of pressure on removal of solid particulates from tar pitch by solvent method. *Chem. Ind. Eng. Prog.* **2021**, *40* (2), 763–770.
- (21) Zhang, D.; Zhang, L.; Fang, X.; Xu, Z.; Sun, X.; Zhao, S. Enhancement of mesocarbon microbead (MCMB) preparation through supercritical fluid extraction and fractionation. *Fuel* **2019**, *237*, 753–762, DOI: [10.1016/j.fuel.2018.10.054](https://doi.org/10.1016/j.fuel.2018.10.054).

- (22) Ye, H.; Jiang, Q.; Sun, H.; Guo, G.; Zhao, L. The Invention Relates to a Pretreatment Process of Raw Asphalt Used for Producing Needle Coke. CN Patent CN201210111167.
- (23) Liu, P.; Zhang, D.; Yang, X.; Cheng, B. An integrated method for preparing low quinoline insoluble modified pitch. *Can. J. Chem. Eng.* **2015**, *93*, 1448–1454, DOI: 10.1002/cjce.22226.
- (24) Li, M.; Zhang, Y.; Yu, S.; Xie, C.; Liu, D.; Liu, S.; Zhao, R.; Bian, B. Preparation and characterization of petroleum-based mesophase pitch by thermal condensation with in-process hydrogenation. *RSC Adv.* **2018**, *8* (53), 30230–30238, DOI: 10.1039/c8ra04679d.
- (25) Hussein, H. Q.; Abdulkarim, A. L. A study of parameters affecting the solvent extraction-flocculation process of used lubricating oil. *J. Eng.* **2023**, *23*, 63–73.
- (26) Manoj, B.; Kunjomana, A. G. Study of stacking structure of amorphous carbon by X-Ray diffraction technique[J]. *Int. J. Electrochem. Sci.* **2012**, *7*, 3127–3134.
- (27) Sonibare, O. O.; Haeger, T.; Foley, S. F. Structural characterization of nigerian coals by X-ray diffraction, Raman and FTIR spectroscopy. *Energy* **2010**, *35* (12), 5347–5353, DOI: 10.1016/j.energy.2010.07.025.
- (28) Nishi, Y.; Mori, N.; Yamada, N.; Inagaki, T. Study on the design method for axial flow runner that combines design of experiments, response surface method, and optimization method to one-dimensional design method. *Renewable Energy* **2022**, *185*, 96–110, DOI: 10.1016/j.renene.2021.12.009.
- (29) Eslami, A.; Asadi, A.; Meserghani, M.; Bahrami, H. Optimization of sonochemical degradation of amoxicillin by sulfate radicals in aqueous solution using response surface methodology (RSM). *J. Mol. Liq.* **2016**, *222*, 739–744, DOI: 10.1016/j.mol-liq.2016.07.096.
- (30) Li, R.; Jiang, Y.; Zhang, Y.; Chen, K.; Huang, B.; Li, L. Optimisation of ammonium sulphate crystallization based on response surface methodology. *J. Chin. Ceram. Soc.* **2022**, *50* (3), 782–790.
- (31) Noordin, M. Y.; Venkatesh, V. C.; Sharif, S.; Elting, S.; Abdullah, A. Application of response surface methodology in describing the performance of coated carbide tools when turning AISI 1045 steel. *J. Mater. Process. Technol.* **2004**, *145* (1), 46–58.
- (32) Ghafari, S.; Aziz, H. A.; Isa, M. H.; Zinatizadeh, A. A. Application of response surface methodology (RSM) to optimize coagulation-flocculation treatment of leachate using poly-aluminum chloride (PAC) and alum. *J. Hazard. Mater.* **2009**, *163* (2–3), 650–656, DOI: 10.1016/j.jhazmat.2008.07.090.
- (33) Yetilmezsoy, K.; Saral, A. Stochastic modeling approaches based on neural network and linear nonlinear regression techniques for the determination of single droplet collection efficiency of countercurrent spray towers. *Environ. Model. Assess.* **2007**, *12* (1), 13–26, DOI: 10.1007/s10666-006-9048-4.
- (34) Jahanbakhshi, A.; Nadooshan, A. A.; Bayareh, M. Multi-objective optimization of microchannel heatsink with wavy microtube by combining response surface method and genetic algorithm. *Eng. Anal. Boundary Elem.* **2022**, *140*, 12–31, DOI: 10.1016/j.engana-bound.2022.04.004.
- (35) Wang, L. *Study on Pretreatment of Medium-Low Temperature Coal Tar Pitch and Preparation of Needle Coke*; Shan Xi: Northwest University: 2019; 20–22.
- (36) Seshadri, K. S.; Albaugh, E. W.; Bacha, J. D. Characterization of needle coke feedstocks by magnetic resonance spectroscopy. *Fuel* **1982**, *61* (4), 336–340, DOI: 10.1016/0016-2361(82)90047-3.
- (37) Zickler, G. A.; Smarsly, B.; Gierlinger, N.; et al. A reconsideration of the relationship between the crystallite size La of carbons determined by X-ray diffraction and Raman spectroscopy. *Carbon* **2006**, *44* (15), 3239–3246, DOI: 10.1016/j.carbon.2006.06.029.
- (38) Morgia, R. Micro-Raman spectroscopy of carbonized semi-fusinite and fusinite. *Int. J. Coal Geol.* **2011**, *87* (3–4), 253–267.
- (39) Rantitsch, G.; Bhattacharyya, A.; Schenk, J.; Lünsdorf, N. K. Assessing the quality of metallurgical coke by Raman spectroscopy. *Int. J. Coal Geol.* **2014**, *130*, 1–7, DOI: 10.1016/j.coal.2014.05.005.
- (40) Li, L.; Lin, X.; Zhang, Y.; Dai, J.; Xu, D.; Wang, Y. Characteristics of the mesophase and needle coke derived from the blended coal tar and biomass tar pitch. *J. Anal. Appl. Pyrolysis* **2020**, *150*, No. 104889, DOI: 10.1016/j.jaap.2020.104889.
- (41) Zhu, Y.; Zhao, X.; Gao, L.; Jun, L.; Cheng, J.; Lai, S. Properties and micro-morphology of primary quinoline insoluble and meso-carbon microbeads. *J. Mater. Sci.* **2016**, *51* (17), 8098–8107, DOI: 10.1007/s10853-016-0080-8.
- (42) Li, L.; Lin, X.; Liu, Z.; Zhang, Y.; Kou, S.; Wang, Y. Identification and quantitative analysis of polarized light micro-structure of coal-derived needle coke. *J. Fuel Chem. Technol.* **2021**, *49* (3), 265–273.